Eur. Phys. J. B (2022) 95:143
https://doi.org/10.1140/epjb/s10051-022-00401-1

THE EUROPEAN PHYSICAL JOURNAL B

Regular Article – Statistical and Nonlinear Physics

# Percolation and jamming properties in particle shape-controlled seeded growth model

D. Dujak[1], A. Karač[2], Lj. Budinski-Petković[3], Z. M. Jakšić[4], and S. B. Vrhovac[4,a]

[1] Faculty of Electrical Engineering, University of Sarajevo, Sarajevo 71000, Bosnia and Herzegovina
[2] Polytechnic Faculty, University of Zenica, Zenica, Bosnia and Herzegovina
[3] Faculty of Engineering, Trg D. Obradovića 6, Novi Sad 21000, Serbia
[4] Institute of Physics Belgrade, University of Belgrade, Pregrevica 118, Zemun, 11080 Belgrade, Serbia

Received 26 May 2022 / Accepted 12 August 2022 / Published online 7 September 2022


**Abstract.** We consider the percolation model with nucleation and simultaneous growth of multiple finite clusters, taking the initial seed concentration $\rho$ as a tunable parameter. Growing objects expand with constant speed, filling the nodes of the triangular lattice according to rules that control their shape. As growing objects of predefined shape, we consider needle-like objects and "wrapping" objects whose size is gradually increased by wrapping the walks in several different ways, making triangles, rhombuses, and hexagons. Growing random walk chains are also analyzed as an example of objects whose shape is formed randomly during the growth. We compare the percolation properties and jamming densities of the systems of various growing shapes for a wide range of initial seed densities $\rho < 0.5$. To gain a basic insight into the structure of the jammed states, we consider the size distribution of deposited growing objects. The presence of the most numerous and the largest growing objects is recorded for the system in the jamming state. Our results suggest that at sufficiently low seed densities $\rho$, the way of the object growth has a substantial influence on the percolation threshold. This influence weakens with increasing $\rho$ and ceases near the value of the site percolation threshold for monomers on the triangular lattice, $\rho_p^* = 0.5$.

## 1 Introduction

The formation of many physical systems can be described by a growth process in which individual elements randomly join together to form an interconnected network. Important examples include the gelation of polymeric materials [1] and the growth of rough surfaces and disorderly interfaces via atomic chemisorption [2]. The most widely used model for such systems is the standard site percolation model, in which each site has a probability $p$ (independent of the neighboring sites) of being designated as occupied or, equivalently, a probability $1-p$ of being designated as empty [3]. Nearest-neighboring occupied sites form structures called clusters. When the probability $p$ exceeds a critical value $p_c$, called the percolation threshold, a spanning cluster occupying a finite fraction of the total number of sites emerges. This infinite cluster corresponds, for example, to a gel in gelation, or to a conduction path through metallic atoms across a surface. The percolation transition is a second-order phase transition and can be characterized by well-defined critical exponents.

More general percolation problems can be formulated by including deposition of extended objects occupying more than one site [4–8]. In random sequential adsorption (RSA) processes particles are randomly, sequentially and irreversibly deposited on an initially empty substrate or lattice with the restriction that they must not overlap with previously added objects [9–12]. The quantity of interest is the fraction of total lattice sites, $\theta(t)$, covered at time $t$ by the deposited objects. Due to the blocking of the substrate area by the previously adsorbed particles, at large times the coverage $\theta(t)$ approaches the jammed-state value $\theta_J$, where only gaps too small to accommodate new particles are left in the monolayer. Percolation assumes the existence of a large cluster that reaches two opposite sides of the lattice [3]. Consequently, $\theta(t)$ ranges from 0 to $\theta_J$ for objects occupying more than one site, so that interplay between RSA and percolation should be considered [13–21]. In Ref. [7] the results for the percolation thresholds, jamming coverages and their ratios were given for the deposition of extended objects on a triangular lattice. It was found that for elongated shapes, the percolation threshold monotonically decreases, while for more compact shapes, it monotonically increases with the object size. For various objects of the same length, the percolation threshold of more compact objects exceeds the perco-

[a] e-mail: vrhovac@ipb.ac.rs (corresponding author)
URL: http://www.ipb.ac.rs/vrhovac/

lation threshold of the elongated ones. Such behavior of the percolation threshold and jamming density as a function of object length is based on simulations for relatively short $k$-mers (up to $k = 20$). Perino *et al.* [22] extended the work of Budinski-Petković *et al.* [7] to larger lattice sizes and longer $k$-mers ($2 \leq k \leq 256$ and $40 \leq L/k \leq 160$). A nonmonotonic size dependence was found for the percolation threshold, which decreases for small objects sizes, goes through a minimum around $k = 13$, and finally increases for larger segments. Furthermore, results suggest that percolation is impossible if $k$ exceeds approximately $10^4$. However, Kondrat *et al.* [16] have refuted these claims and presented rigorous proof that each cluster in every jammed configuration of fixed-length nonoverlapping horizontal or vertical needles on a finite square lattice is a percolating cluster. Slutskii *et al.* [17] have generalized this theorem to the case of periodic boundary conditions.

Standard percolation usually deals with the problem when the constitutive elements of the clusters are randomly distributed. However, correlations cannot always be ignored when, for example, percolation follows a particular direction along which activity can spread only in one way. Several correlated percolation models such as bootstrap percolation [23], directed percolation [24], and spiral percolation [25] are studied extensively.

In the past two decades, it has become possible to synthesize many classes of nanoscale building blocks with controlled structure, size, and shape for applications in electronics, photonics, chemical engineering, medicine, etc. However, researchers must solve the fundamental problem of how to use nanoscale blocks to build functional structures or devices. Assembly of building blocks for large-scale applications, therefore, appears as fundamental problems of contemporary nanotechnology. Seeded growth has emerged as a compelling method to create a wide variety of novel metal nanostructures [26–28]. Seeded methods are outstanding way to obtain high-quality nanocrystal samples because structurally well-defined seeds can be selected and serve as preferential platforms for deposition of additional material [28–30].

We propose an artificial, but instructive model which is able to reproduce the granular growth, from nucleation to percolation and for different growing shapes. This model can be regarded as a very simple picture of the size- and shape-controlled nano-particles growth. Actually, we examine numerically a percolation model with nucleation and simultaneous growth of multiple finite clusters, taking the initial seed concentration $\rho$ as a tunable parameter [31–33]. However, growth of islands is now deterministic rather than stochastic. Objects expand with constant speed, incorporating and filling the nodes of the triangular lattice according to a predefined rules that determine their shape. As growing objects of fixed shape, we consider needle-like objects, and "wrapping" objects which size is gradually increased by wrapping the walks in several different ways, making triangles, rhombuses and hexagons. In addition, growing random walk chains are also analyzed as an example of objects whose shape is formed

**Table 1** Wrapping triangles, $T_j$. The colors are associated with different order $n_s$ of the symmetry axis

| Shape ($T_j$) | $j$ | $n_s$ | $\theta_J$ |
|---|---|---|---|
|  | 2 | 2 | 0.9141(3) |
|  | 3 | 3 | 0.7970(4) |
|  | 4 | 1 | 0.7741(4) |
|  | 5 | 1 | 0.7605(4) |
|  | 6 | 3 | 0.7211(5) |
|  | 7 | 1 | 0.6901(5) |
|  | 8 | 1 | 0.6993(5) |
|  | 9 | 1 | 0.7101(4) |
|  | 10 | 3 | 0.6816(6) |
|  | 11 | 1 | 0.6493(5) |
|  | 12 | 1 | 0.6624(5) |
|  | 13 | 1 | 0.6683(6) |
|  | 14 | 1 | 0.6816(7) |
|  | 15 | 3 | 0.6572(6) |
| 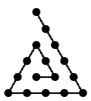 | 16 | 1 | 0.6263(7) |
| 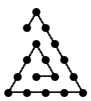 | 17 | 1 | 0.6368(7) |
|  | 18 | 1 | 0.6445(6) |
|  | 19 | 1 | 0.6518(6) |
|  | 20 | 1 | 0.6633(6) |
|  | 21 | 3 | 0.6406(8) |
| 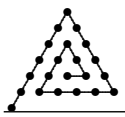 | 22 | 1 | 0.6119(8) |

**Table 1** continued

| Shape ($T_j$) | $j$ | $n_s$ | $\theta_J$ |
|---|---|---|---|
| 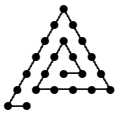 | 23 | 1 | 0.6197(9) |
| 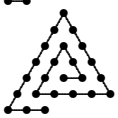 | 24 | 1 | 0.6286(8) |
| 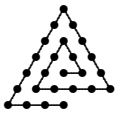 | 25 | 1 | 0.6323(8) |
| 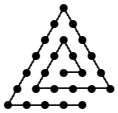 | 26 | 1 | 0.6406(9) |
| 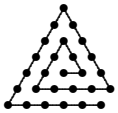 | 27 | 1 | 0.6498(7) |
| 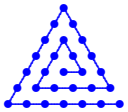 | 28 | 3 | 0.6286(7) |
| 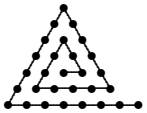 | 29 | 1 | 0.6016(9) |
| 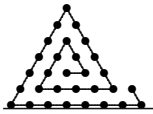 | 30 | 1 | 0.6079(10) |

For each shape, $\theta_J$ is the jamming coverage. The numbers in parentheses are the numerical values of the standard uncertainty of $\theta_J$ referred to the last digits of the quoted value

randomly during the growth. We compare the percolation properties and jamming densities of the systems of growing needle-like objects ($k$-mers), wrapping shapes, and growing self-avoiding random walks for a wide range of initial seed densities $\rho$. To gain a basic insight into the structure of the jammed state, we consider the size distribution of deposited growing objects. Length of the most numerous and the length of the largest growing objects in the jamming coverages are also examined for whole range of initial seed densities $\rho < 0.5$. The presented results suggest that at sufficiently low seed densities $\rho$, the way of the object growth has a substantial influence on the percolation threshold. This influence weakens with increasing $\rho$ and ceases near to the value of the site percolation threshold for monomers on the triangular lattice, $\rho_p^* = 0.5$ [34].

The paper is organized as follows. Section 2 describes the details of the model and the numerical simulations. The results of the simulations for growing objects of various shapes are given in Sect. 3. Finally, Sect. 4 contains some additional comments and final remarks.

**Table 2** Wrapping rhombuses, $R_j$. The colors are associated with different order $n_s$ of the symmetry axis

| Shape ($R_j$) | $j$ | $n_s$ | $\theta_J$ |
|---|---|---|---|
|  | 2 | 2 | 0.9141(3) |
|  | 3 | 1 | 0.8345(3) |
|  | 4 | 2 | 0.7591(4) |
|  | 5 | 1 | 0.7605(4) |
|  | 6 | 2 | 0.7299(4) |
|  | 7 | 1 | 0.7075(5) |
|  | 8 | 1 | 0.6956(5) |
|  | 9 | 2 | 0.6793(6) |
|  | 10 | 1 | 0.6706(6) |
|  | 11 | 1 | 0.6885(5) |
|  | 12 | 2 | 0.6716(6) |
|  | 13 | 1 | 0.6506(7) |
|  | 14 | 1 | 0.6531(6) |
|  | 15 | 1 | 0.6463(6) |
|  | 16 | 2 | 0.6428(7) |
|  | 17 | 1 | 0.6332(7) |
|  | 18 | 1 | 0.6439(8) |
| 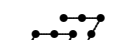 | 19 | 1 | 0.6549(7) |
|  | 20 | 2 | 0.6416(6) |
|  | 21 | 1 | 0.6224(8) |
|  | 22 | 1 | 0.6258(8) |
|  | 23 | 1 | 0.6254(7) |
| 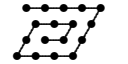 | 24 | 1 | 0.6226(7) |
| 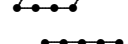 | 25 | 2 | 0.6220(7) |

**Table 2** continued

| Shape ($R_j$) | $j$ | $n_s$ | $\theta_J$ |
|---|---|---|---|
|  | 27 | 1 | 0.6199(9) |
|  | 28 | 1 | 0.6260(9) |
| 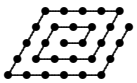 | 29 | 1 | 0.6349(10) |
| 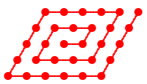 | 30 | 2 | 0.6236(9) |

For each shape, $\theta_J$ is the jamming coverage. The numbers in parentheses are the numerical values of the standard uncertainty of $\theta_J$ referred to the last digits of the quoted value

## 2 Definition of the model and the simulation method

The model is developed on a triangular lattice of size $L$ in two dimensions (2D) with periodic boundary conditions. The lattice is initially and randomly occupied by point-like seeds at given concentration $\rho$ less than $\sim 0.5$. This concentration is defined as a fraction of sites of the lattice that are occupied by seeds. For each seed, a grain, composed by self-avoiding lattice steps, grows. Note that there are multiple growth centers from which finite clusters grow simultaneously.

The growing objects are modeled by self-avoiding steps on the planar triangular lattice. A self-avoiding shape of length $\ell$ is a sequence of *distinct* vertices $(\omega_0, \ldots, \omega_l)$ such that each vertex is a nearest neighbor of its predecessor, i.e., a walk of length $\ell$ covers $j = \ell+1$ lattice sites. We consider three different types of growing shapes: needle-like objects, random walk chains, and wrapping shapes. Needle-like shapes are $k$-mers of length $\ell = k - 1$. Chains are formed by self-avoiding *random* walks (SARW), which are generated under the simple constraint that step $i + 1$ cannot return to the location of the walk at step $i$. The wrapping shapes are made by self-avoiding lattice steps in a specific manner. Starting from a monomer ($\ell = 0$), size of the objects is gradually increased by wrapping the walks in several different ways. Formation of wrapping triangles $T_j$ is shown in Table 1. In a similar way, rhombuses $R_j$ and hexagons $H_j$ of larger sizes are obtained by wrapping as shown in Tables 2 and 3 , respectively. In this manner, wrapping objects of larger sizes occupy all comprised sites on the lattice.

The initial state of the system is prepared through the random sequential adsorption model (RSA) of seeds in two dimensions. For this purpose, we perform the Monte Carlo procedure of filling the triangular lattice by inserting the monomers randomly, up to the chosen coverage fraction $\rho$. In this way, we are able to prepare

**Table 3** Wrapping hexagons, $H_j$. The colors are associated with different order $n_s$ of the symmetry axis

| Shape ($H_j$) | $j$ | $n_s$ | $\theta_J$ |
|---|---|---|---|
|  | 2 | 2 | 0.9141(3) |
|  | 3 | 3 | 0.7970(4) |
|  | 4 | 2 | 0.7591(4) |
|  | 5 | 1 | 0.7605(4) |
|  | 6 | 1 | 0.7347(4) |
|  | 7 | 6 | 0.6696(5) |
|  | 8 | 1 | 0.6923(5) |
|  | 9 | 1 | 0.6857(5) |
|  | 10 | 2 | 0.6813(4) |
|  | 11 | 1 | 0.6665(6) |
|  | 12 | 3 | 0.6508(5) |
|  | 13 | 1 | 0.6431(5) |
|  | 14 | 2 | 0.6457(6) |
|  | 15 | 1 | 0.6433(7) |
|  | 16 | 1 | 0.6623(6) |
|  | 17 | 1 | 0.6472(6) |
|  | 18 | 1 | 0.6367(7) |
|  | 19 | 6 | 0.6148(6) |
| 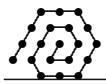 | 20 | 1 | 0.6163(7) |

**Table 3** continued

| Shape ($H_j$) | $j$ | $n_s$ | $\theta_J$ |
|---|---|---|---|
|  | 21 | 1 | 0.6352(6) |
|  | 22 | 1 | 0.6265(8) |
|  | 23 | 1 | 0.6293(8) |
|  | 24 | 2 | 0.6327(9) |
|  | 25 | 1 | 0.6204(8) |
|  | 26 | 1 | 0.6190(10) |
|  | 27 | 3 | 0.6136(9) |
|  | 28 | 1 | 0.6057(10) |
| 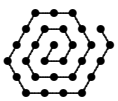 | 29 | 1 | 0.6099(10) |
| 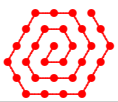 | 30 | 2 | 0.6119(12) |

For each shape, $\theta_J$ is the jamming coverage. The numbers in parentheses are the numerical values of the standard uncertainty of $\theta_J$ referred to the last digits of the quoted value

the system in disordered initial state with a statistically reproducible density $\rho$. Then, for each initially prepared configuration, we switch the deposition events off and initiate a random growing processes in our system.

At each Monte Carlo step, a lattice site occupied by a seed is selected at random. The first segment of a growing object is formed by randomly selecting an adjacent node that is not occupied by another seed or object. We allow only the single step object growth that do not cause a double occupation at any site. If the selected seed is the beginning of a non-zero length object, only the last point of the corresponding self-avoiding walk is active for further growth. In the case of needle-like shapes, the chosen $k$-mer ($k > 1$) grows in direction of the first step in the formation of the shape on the lattice. If the corresponding adjacent site is not empty, the attempted $k$-mer elongation is not possible and the object remains unchanged. In the case of random walk chains, the object growth depends on the occupancy of the first neighbors of the last point of the walk. If there are no empty nearest neighbors of the ending site of the walk, the chosen chain does not change. If the ending site has empty adjacent sites, the selected chain randomly extends into one of them. Growing of wrapping triangles, rhombuses and hexagons depends in the same way on the occupancy of the first neighbors of the ending site, but the rules of their growth are illustrated in the Tables 1, 2 and 3 , respectively.

**Table 4** The jamming coverages $\theta_J$ and the percolation thresholds $\theta_p^*$ for $k$-mers of different lengths $\ell = k - 1$

| $k$-mer | $\ell$ | $\theta_J$ | $\theta_p^*$ |
|---|---|---|---|
|  | 0 | 1 | 0.5000(1) |
|  | 1 | 0.9141(3) | 0.4867(1) |
|  | 2 | 0.8362(4) | 0.4628(3) |
|  | 3 | 0.7891(6) | 0.4432(2) |
|  | 4 | 0.7584(7) | 0.4299(4) |
|  | 5 | 0.7370(9) | 0.4206(5) |
|  | 6 | 0.7212(11) | 0.4145(6) |
|  | 7 | 0.7089(12) | 0.4124(6) |

The numbers in parentheses are the numerical values of the standard uncertainty of $\theta_J$ and $\theta_p^*$ referred to the last digits of the quoted value

During the growth of the objects, if two objects come in contact, i.e., are found to be separated by a single lattice spacing, they are merged into a single cluster. During the growth of these clusters, two clusters may come in contact. Two clusters with occupied perimeter sites separated by a single lattice spacing is amalgamated to be a single cluster. Consequently, the coverage of the lattice is increased in the process up to the percolation threshold $\theta_p$, when there appears a cluster that extends through the whole system. We say that a percolating cluster arises in the system when the opposite edges of the system are connected via some path of nearest neighbor sites occupied by the particles. The tree-based union/find algorithm was used to determine the percolation threshold $\theta_p$ [35].

Another quantity of interest is the jamming coverage $\theta_J$. In standard lattice RSA problems jamming coverage $\theta_J$ is reached when no more objects can be placed in any position on the lattice [36,37]. The jamming density values corresponding to the random deposition of triangles, rhombuses and hexagons are given in the Tables 1, 2 and 3 , respectively. In the present case, jamming limit $\theta_J$ is reached when no more growing objects can be increased in any necessary direction on the lattice. Additionally, in Table 4 we show the jamming coverages $\theta_J$ and the percolation thresholds $\theta_p^*$ for $k$-mers of different lengths $\ell = k - 1 = 0, \ldots, 7$ [34]. These

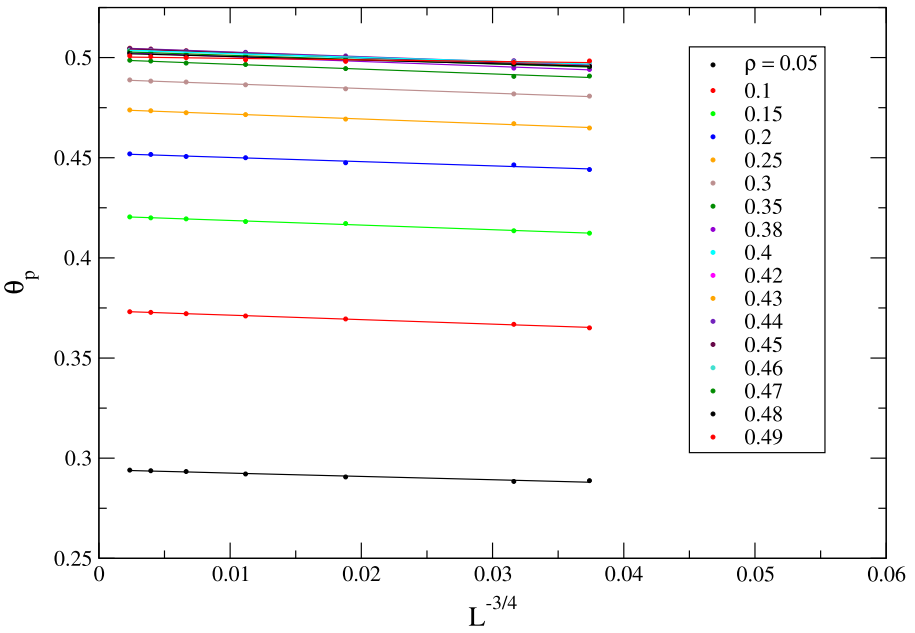


**(a)**

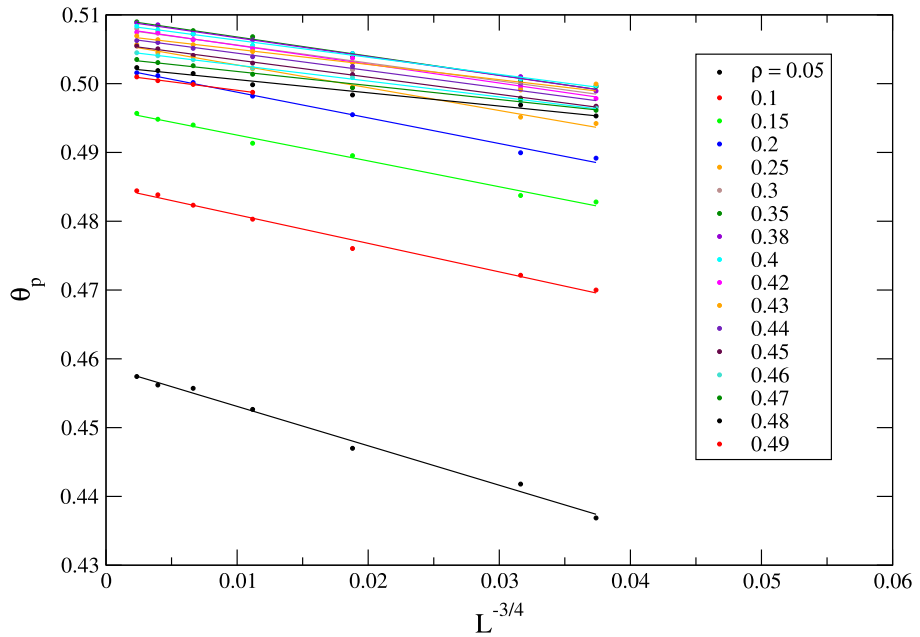


**(b)**

**Fig. 1** Finite-size scaling of the effective percolation threshold $\theta_{\mathrm{p}}$ against $L^{-1/\nu}$ with $\nu = 4/3$ for (**a**) growing needle-like objects, and (**b**) growing random walk chains, for various values of the initial seed densities $0.05 \leq \rho \leq 0.49$

values are in a very good agreement with the results published in [22].

## 3 Results and discussion

Percolation thresholds and jamming densities are obtained for growing objects for a wide range of initial seed densities $\rho < 0.5$. Values of the percolation thresholds for the infinitely large lattice $\theta_{\mathrm{p}}^{*}$ are obtained using the usual finite-size scaling analysis of the percolation behavior on two-dimensional lattices [3]. In such systems, one assumes that the effective percolation threshold $\theta_{\mathrm{p}}$ (the mean value of threshold measured for a finite lattice) approaches the asymptotic value $\theta_{\mathrm{p}} \to \theta_{\mathrm{p}}^{*}$ for $L \to \infty$ via the power law:

$$\theta_{\mathrm{p}} - \theta_{\mathrm{p}}^{*} \propto L^{-1/\nu} \,. \tag{1}$$

Here, the constant $\nu$ is the critical exponent that governs the divergence of the correlation length as $\xi \propto |\theta_p - \theta_p^*|^{-\nu}$. It should be noticed that the universality class of random percolation in two dimensions is very well identified and the critical exponents are known exactly, namely, $\nu = 4/3$ [3]. The latter relationship allows us to extrapolate the threshold for an infinite system, $L \to \infty$. Simulations were performed for lattices of various sizes ranging from $L = 40$ to $L = 3200$ and the data are averaged over 500 independent runs for each lattice size.

Plotting the mean value $\theta_p$ of the threshold for various lattice sizes against $L^{-1/\nu}$, we confirm the validity of the finite-size scaling in the system and determine the asymptotic value of the percolation threshold $\theta_p^*$. Finite-size scaling of the lattice threshold $\theta_p$ against $L^{-1/\nu}$ ($\nu = 4/3$) for needle-like objects and random walk chains is illustrated in Fig. 1a,b, respectively, for various initial seed densities $0.05 \le \rho \le 0.49$.

In Fig. 2, we show the typical snapshot configurations at (a) the beginning of the process ($\theta = \rho = 0.35$), (b) percolation threshold ($\theta = \theta_p^*$), and (c) jamming state ($\theta = \theta_J$), obtained for wrapping triangles. The snapshots of size $\Delta L^2 = 32^2$ are taken from the central part of the lattice. The colors of the lattice nodes are determined by the size of the growing object in them.

Dependence of the percolation threshold $\theta_p^*$ on the initial seed (monomer) density $\rho$ is shown in Fig. 3 for growing needle-like objects ($k$-mers) and growing random walk chains. In both cases, the percolation threshold $\theta_p^*$ grows monotonically for sufficiently low values of initial seed density $\rho$. At low values of initial monomer densities objects have enough space to grow, surface is porous, and the percolation threshold $\theta_p^*$ is reached at low values of the coverage. Higher initial monomer density suppresses the object growth. As the seed density increases, the contribution of small objects in the coverage increases and the percolation threshold $\theta_p^*$ is reached at higher coverages. Percolation thresholds $\theta_p^*$ for the growing random walks chains are higher than those for the growing needle-like objects, especially at low seed densities. During the object growth, the random walk chains cover the surface more efficiently than $k$-mers and the percolation occurs at higher coverage values. It is interesting that the percolation threshold $\theta_p^*$ after growth at lower density values $\rho$, reaches a broad maximum, and slightly falls for larger $\rho$, as shown in the inset of Fig. 3. Indeed, at sufficiently high initial seed densities $\rho$, slight growth of objects is sufficient for their connection and efficient propagation of clusters. At densities $\rho$ close to the percolation threshold for monomers ($\rho_p^* = 0.5$), the growth of objects up to the short $k$-mers (e.g., dimers or 3-mers) can ensure the formation of a percolation cluster. This is the reason for the small difference in percolation thresholds between the growing needle-like objects and the growing random walk chains when the density of the seeds is close to $\rho_p^* = 0.5$.

Values of the jamming coverage $\theta_J$ are shown in Fig. 4 for the growing needle-like objects and the growing ran-

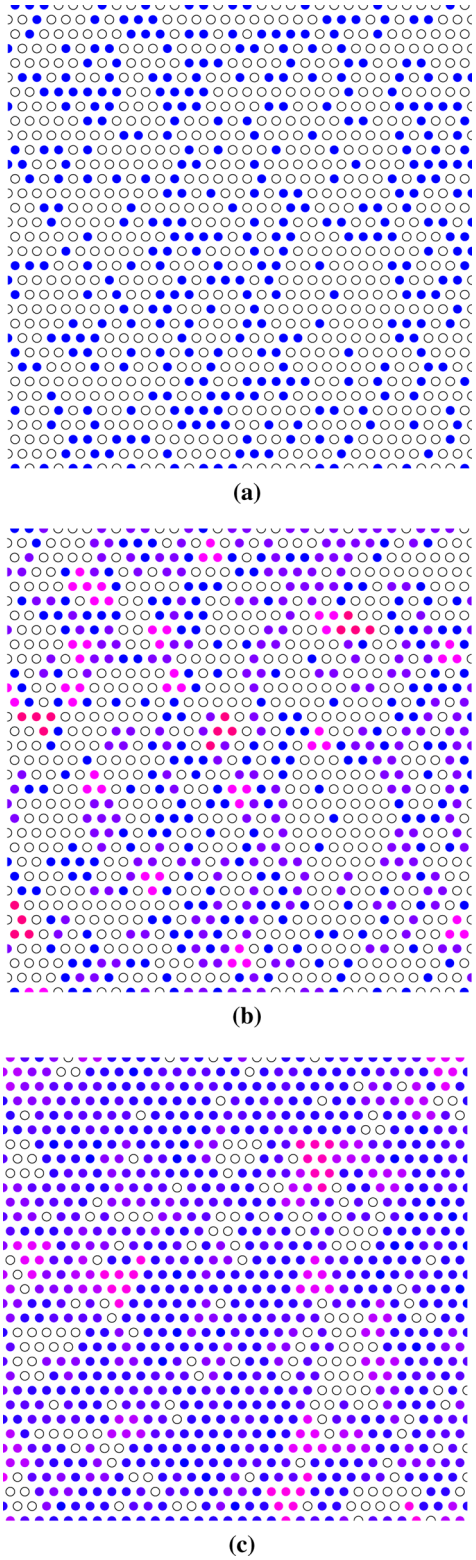


**Fig. 2** Typical configurations of wrapping triangles at (**a**) $\theta = \rho$, (**b**) $\theta = \theta_p^*$, and (**c**) $\theta = \theta_J$ obtained for initial seed (monomer) density $\rho = 0.35$. The snapshots are taken from the central part of the packings. Colormap "blue–purple–pink–red" corresponds to the size distribution of growing objects, from the smaller to the larger ones

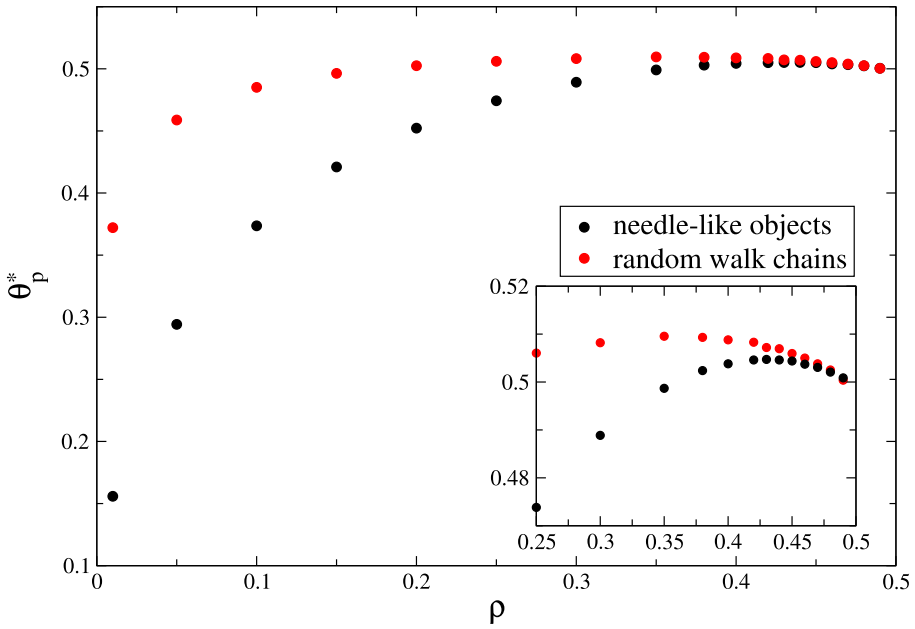


**Fig. 3** Dependence of the percolation threshold $\theta_p^*$ on the initial seed density $\rho$ for growing needle-like objects (black symbols) and growing random walk chains (red symbols). The inset shows an enlarged part of this graph that displays a non-monotonic behavior

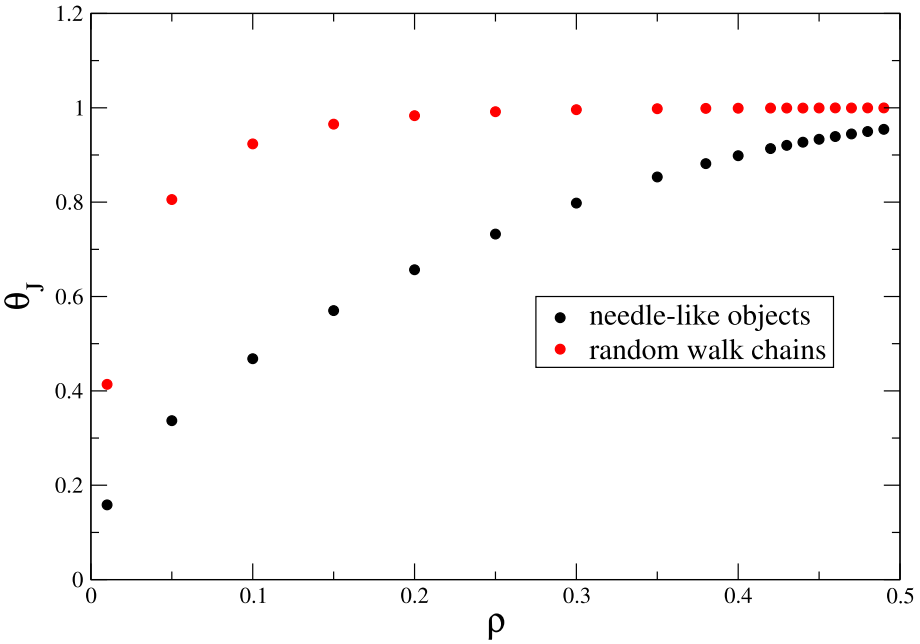


**Fig. 4** Dependence of the jamming density $\theta_J$ on the initial seed density $\rho$ for growing needle-like objects (black symbols) and growing random walk chains (red symbols)

dom walk chains. Jamming coverage $\theta_J$ grows with the initial seed density $\rho$ for both ways of the object growth. Growing self-avoiding random walks cover the surface more efficiently than the growing $k$-mers so that $\theta_J$ has higher values for the first one, for all investigated seed densities $\rho$.

To gain a basic insight into the structure of coverings generated by the process of the object growth, we first consider the number of deposited $k$-mers $N(k)$, $k \geq 1$, normalized by the initial number of seeds $N_0$. Dependence of the ratio $N(k)/N_0$ on the object length $\ell = k - 1$ for the system in the jamming state is shown in Fig. 5 for various values of the seed density $\rho$. For all presented initial seed densities $\rho \geq 0.1$, maximum of the ratio $N(k)/N_0$ is for the length equal unity, i.e., dimers are the most numerous objects in the deposit at the jamming coverage. Only for the very low initial monomer densities, such as $\rho = 0.01$ and $\rho = 0.05$,

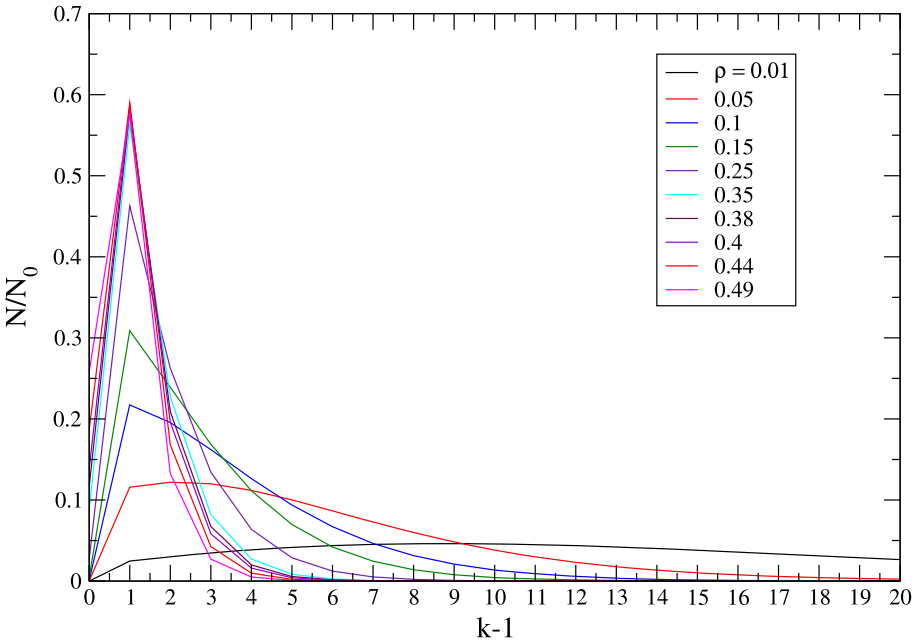


**Fig. 5** Dependence of the normalized number of deposited $k$-mers $N(k)/N_0,\ k \geq 1$ on the object length $\ell = k - 1$, for the system in the jamming state. Curves are given for various values of seed density $\rho$, as indicated in the legend. Here, $N_0$ is initial number of seeds at given density $\rho$

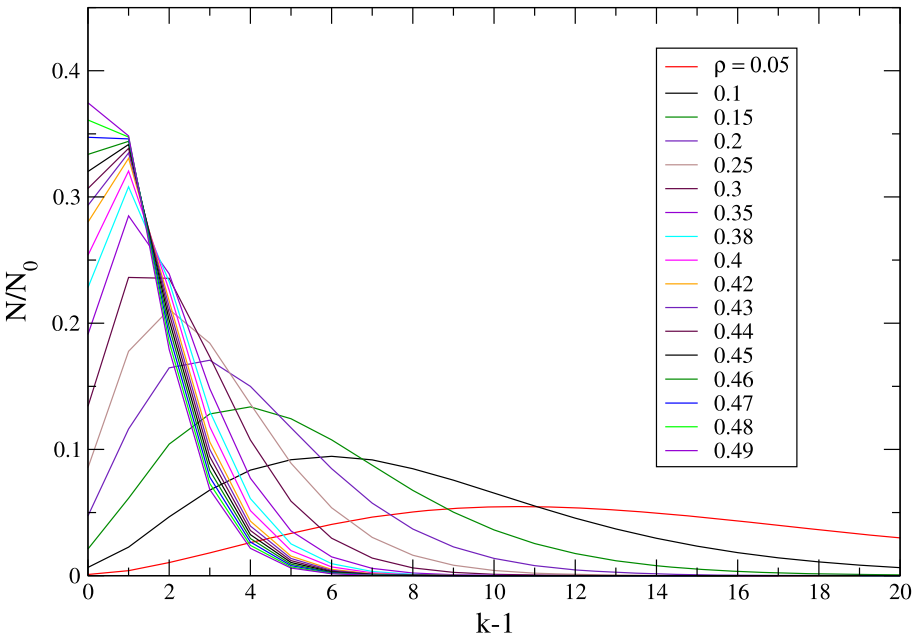


**Fig. 6** Dependence of the normalized number of growing random walk chains $N(\ell)/N_0$ on the walk length $\ell = k - 1$, for the system in the jamming state. Curves are given for various values of seed density $\rho$, as indicated in the legend. Here, $N_0$ is initial number of seeds at given density $\rho$

longer $k$-mers prevail in the jamming configuration. In Fig. 6, normalized number $N(\ell)/N_0$ of the growing random walk chains *vs.* their length $\ell$, for various values of the initial seed densities $\rho$ is presented. For the highest seed densities $\rho$, most of the initial monomers do not even start their growth, they are followed in number by walks cowering two lattice sites, and the ratio $N(\ell)/N_0$ decreases with the length $\ell$ of the self-avoiding random walks. At the initial monomer densities between $\rho = 0.3$ and $\rho = 0.46$ maximum of the ratio $N(\ell)/N_0$ is reached by the walks cowering two lattice sites. Furthermore, for lower initial monomer densities, this maximum is shifted towards longer self-avoiding random walks.

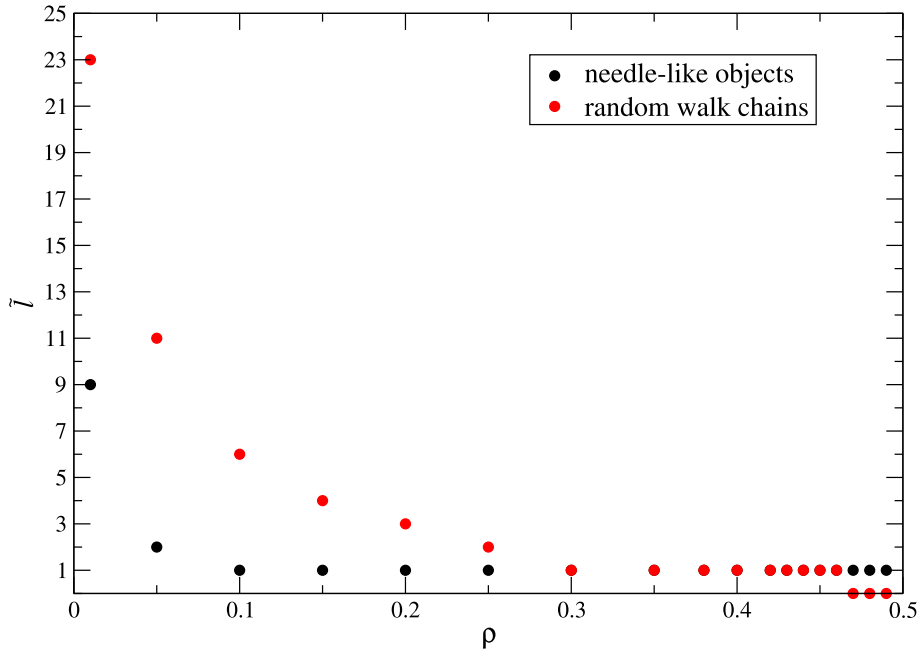


**Fig. 7** Length $\tilde{\ell}$ of the most numerous growing objects in the jamming coverages *vs.* the initial seed density $\rho$. Results are given for growing needle-like objects ($k$-mers) and for growing random walk chains, as indicated in the legend

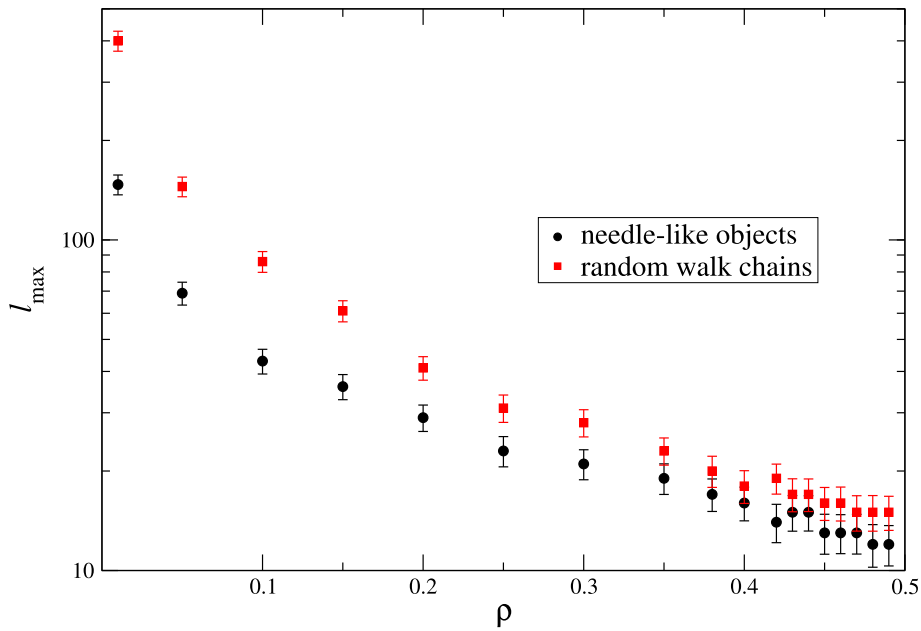


**Fig. 8** Length $\ell_{\max}$ of the largest growing objects in the jamming coverages *vs.* the initial seed density $\rho$. Results are given for growing needle-like objects ($k$-mers) and for growing random walk chains, as indicated in the legend. The error bars represent the standard deviation

Length $\tilde{\ell}$ of the most numerous growing object in the jamming coverages depends on the initial seed density $\rho$. These dependencies for the cases of the growing needle-like objects and the growing random walk chains are given in Fig. 7. It can be seen that for values of the initial seed densities over $\rho = 0.1$ the most numerous growing $k$-mers are dimers. However, at very low values of $\rho$, the most numerous $k$-mers appear to be longer since $k$-mers have more space for growth. At low initial monomer densities $\rho$, the growing random walk chains can reach larger lengths than the $k$-mers. The difference in the length of the most numerous objects between the $k$-mers and the random walk chains decreases with $\rho$. For $0.3 \leq \rho \leq 0.46$, the most numerous random walk chains are covering two lattice sites ($\tilde{\ell} = 1$). For larger values of $\rho > 0.46$, the most numerous objects are monomers ($\tilde{\ell} = 0$) because a large part of seeds cannot start their growth at such high densities.

**Table 5** Values of the jamming coverages $\theta_J$ and the percolation thresholds $\theta_p^*$ for compact triangles $T_j$, rhombuses $R_j$, and hexagons $H_j$ of larger sizes

| $(x_j)$ | Shape | $\theta_J$ | $\theta_p^*$ |
|---|---|---|---|
| $(T_3)$ |  | 0.7970(4) | 0.5214(9) |
| $(T_6)$ |  | 0.7211(5) | 0.5524(14) |
| $(T_{10})$ |  | 0.6816(6) | 0.5789(15) |
| $(T_{15})$ | . . . | 0.6572(6) | 0.6003(15) |
| $(T_{21})$ | . . . | 0.6406(8) | / |
| $(T_{28})$ | . . . | 0.6286(7) | / |
| $(R_4)$ |  | 0.7591(4) | 0.5393(12) |
| $(R_9)$ |  | 0.6793(6) | 0.5793(14) |
| $(R_{16})$ | . . . | 0.6428(7) | / |
| $(R_{25})$ | . . . | 0.6220(7) | / |
| $(H_7)$ |  | 0.6696(5) | 0.5843(13) |
| $(H_{19})$ | 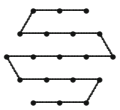 | 0.6148(6) | / |
| $(H_{37})$ | . . . | 0.5942(8) | / |

For larger sizes of compact objects a no-percolation regime is observed. The numbers in parentheses are the numerical values of the standard uncertainty of $\theta_J$ and $\theta_p^*$ referred to the last digits of the quoted value

Figure 8 shows the dependences of the length $\ell_{max}$ of the largest growing objects in the jamming coverages on the initial seed density $\rho$. These dependencies are given for the cases of growing needle-like objects and growing random walk chains. Due to the flexibility of the self-avoiding random walks, for all initial monomer densities $\rho$, the growing random walk chains can reach larger lengths than the growing $k$-mers. This difference is most pronounced for the lowest values of $\rho$ and decreases with increasing initial monomer density $\rho$.

Simulations are also performed for the wrapping triangles, rhombuses and hexagons shown in Tables 1–3. In Table 5, we show the values for the jamming density $\theta_J$ and the percolation threshold $\theta_p^*$ for several regular triangles, rhombuses, and hexagons of various sizes. Interestingly, compact objects of larger sizes can show a no-percolating behavior on the triangular lattice [7,8,38]. In Table 5, we present only the percolation thresholds for the objects for which percolation was reached in all $N = 500$ runs on the largest lattice used in the finite-size scaling analysis ($L = 3200$). This effect is most pronounced for hexagons for which no percolation was found for the objects larger than the basic ones. Our results are in a good agreement with the results presented in reference [5], where the maximal length for which the most bent particles percolate is $a = 13$; while for the not fully bent particles, the maximal length is about $a = 22$. The absence of percolation has also been reported in the studies of RSA of large rectangular particles [39], squares [40], and bent particles [5] on a square lattice.

Finite-size scaling of the percolation threshold $\theta_p$ against $L^{-1/\nu}$, with $\nu = 4/3$, is illustrated in Fig. 9 for the growing triangles, rhombuses and hexagons. Results are presented for various initial seed densities ranging from $\rho = 0.15$ to $\rho = 0.49$. Values of the percolation thresholds $\theta_p^*$ obtained by the extrapolation for an infinite lattice ($L \to \infty$) are presented in Fig. 10. We can see that the dependence of $\theta_p^*$ on the initial seed density $\rho$ differs significantly for these three ways of the object growth, especially for lower densities $\rho$. At lower densities, objects can reach larger sizes and the diversity of shapes has a significant influence on making bonds leading to percolation. At high seed densities $\rho$, a great majority of objects are small with few shape variations, and the percolation thresholds have similar values for different types of wrapping shapes.

Values of the jamming coverages $\theta_J$ for wrapping triangles, rhombuses and hexagons *vs.* the seed density $\rho$ are shown in Fig. 11. It is interesting to note that these jamming coverages differ only slightly for different ways of the object growth. This can be explained by the fact that the small empty regions in the finale stages of the process are filled with the smallest objects.

Figure 12 shows the dependences of the length $\ell_{max}$ of the largest wrapping objects in the jamming coverages on the initial seed density $\rho$. For low values of the seed density $\rho$, the largest wrapping triangles, rhombuses and hexagons can reach rather large sizes at jamming density $\theta_J$. The number of sites $\ell_{max}$ covered by the largest growing object in the jamming configuration decreases with the initial monomer density $\rho$.

## 4 Concluding remarks

Jamming and percolation of growing objects was investigated for needle-like objects, random walk chains and wrapping shapes—triangles, rhombuses and hexagons. Simulations were performed for initial states of various initial seed densities $\rho < 0.5$.

Jamming coverage $\theta_J$ increases with the initial seed density $\rho$ for all examined ways of the object growth. Comparing the growing needle-like objects and the random walk chains, jamming densities $\theta_J$ has larger values for the latter ones for all initial seed densities. Values of the jamming coverages $\theta_J$ for the wrapping triangles, rhombuses and hexagons differ only slightly for differ-

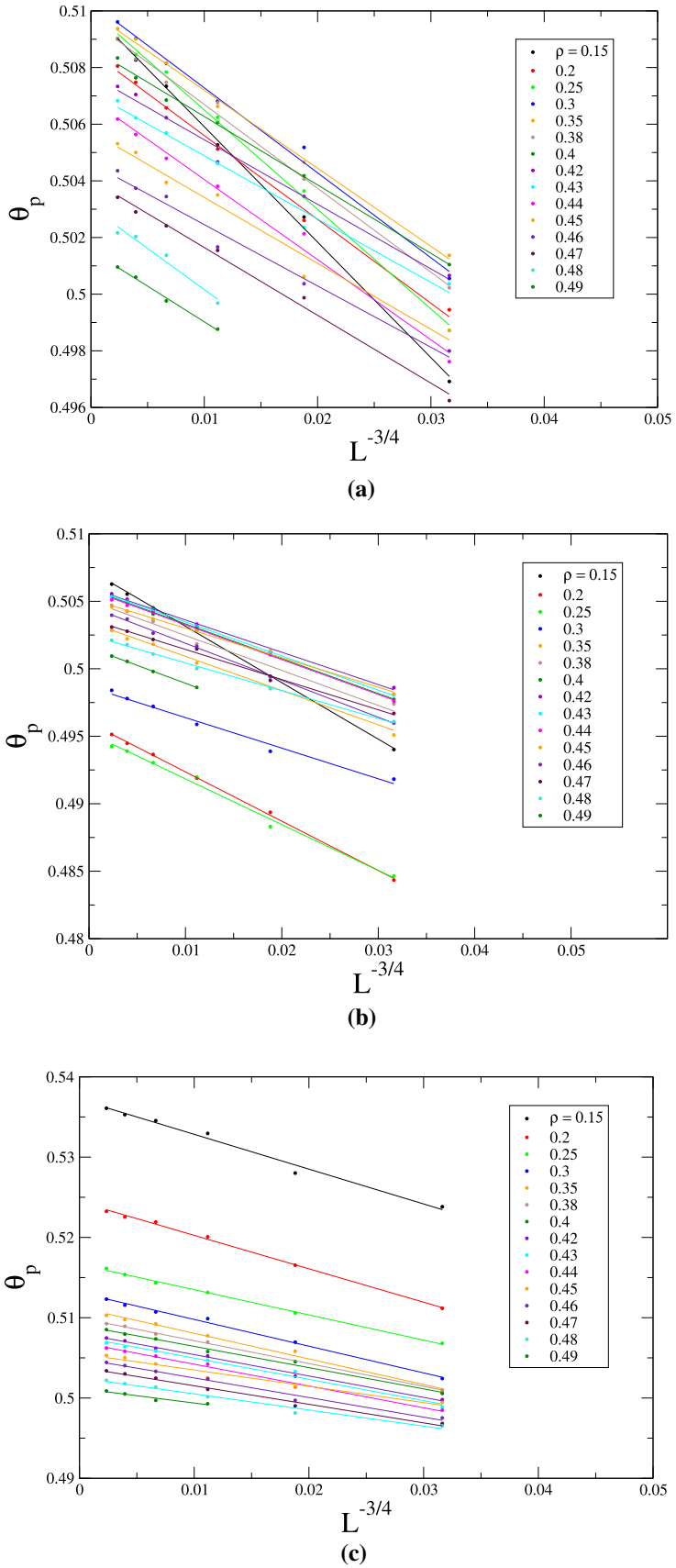


**Fig. 9** Finite-size scaling of the effective percolation threshold $\theta_{\mathrm{p}}$ against $L^{-1/\nu}$ with $\nu = 4/3$ for wrapping (**a**) triangles, (**b**) rhombuses, and (**c**) hexagons, for various values of the initial seed densities $0.15 \leq \rho \leq 0.49$

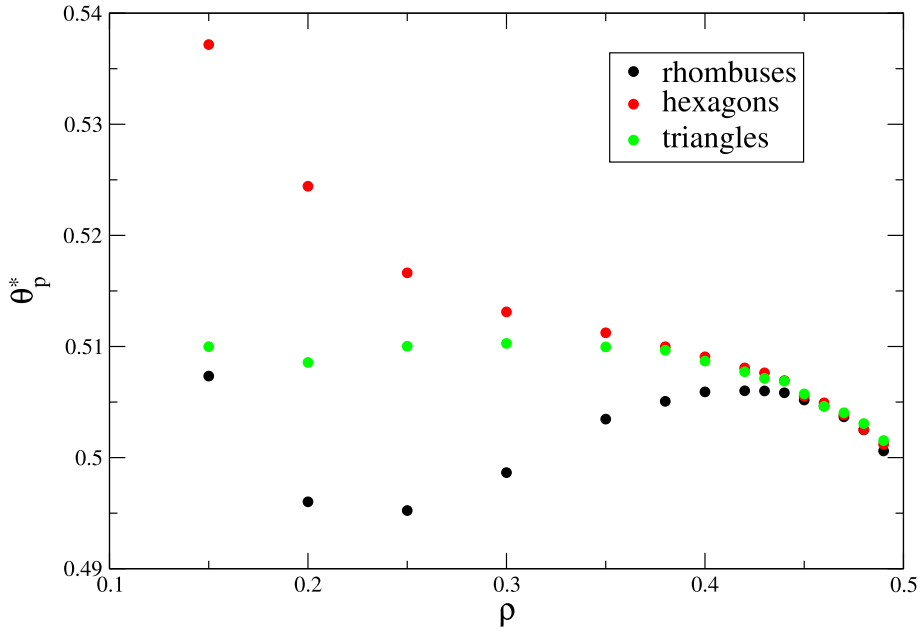


**Fig. 10** Dependence of the percolation threshold $\theta_p^*$ on the initial seed density $\rho$ for wrapping triangles (green), rhombuses (black), and hexagons (red)

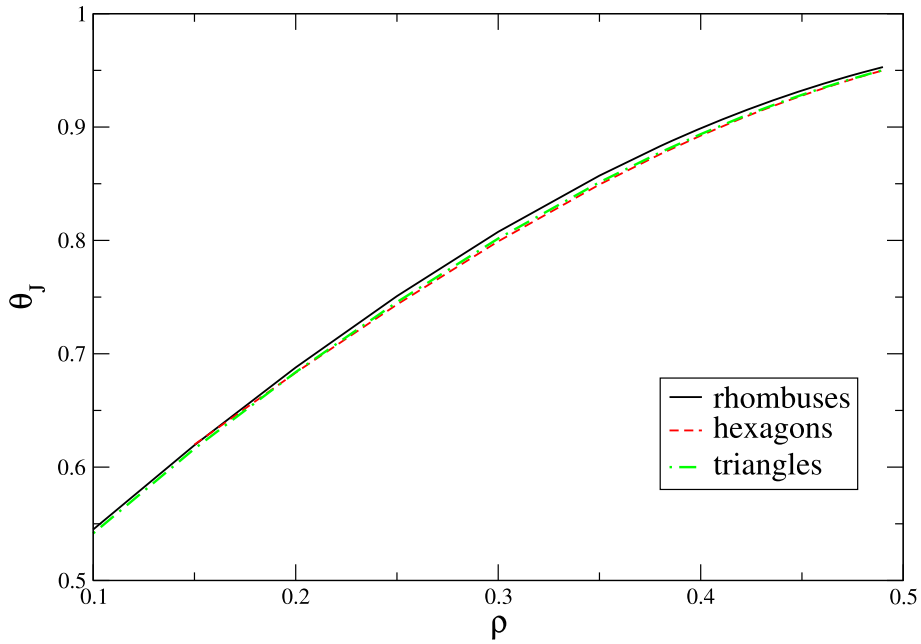


**Fig. 11** Dependence of the jamming density $\theta_J$ on the initial seed density $\rho$ for wrapping triangles (green), rhombuses (black), and hexagons (red)

ent ways of the object growth. It is interesting to note that $\theta_J$ of the wrapping objects is lower than $\theta_J$ of the needle-like objects at low seed densities, and it is even higher than $\theta_J$ of the random walk chains for very high values of $\rho$. At higher seed densities $\rho$, the most numerous objects in the jamming configurations are dimers, and even monomers. Longer objects prevail at lower initial densities.

For the growing needle-like objects and the growing random walk chains, the percolation threshold $\theta_p^*$ increases with $\rho$ for lower values of the initial seed density, reaches a broad maximum, and slightly falls for higher values of $\rho$. The growing random walk chains cover the surface more efficiently than the needle-like objects and percolation is reached at higher coverages for the random walk chains.

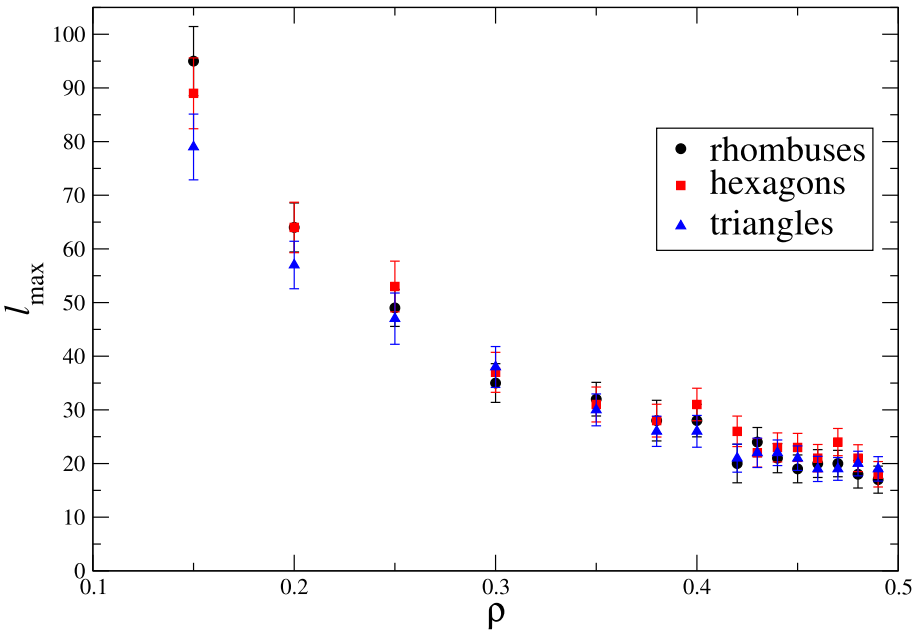


**Fig. 12** Length $\ell_{\max}$ of the largest growing objects in the jamming coverages *vs.* the initial seed density $\rho$. Results are given for wrapping triangles, rhombuses, and hexagons, as indicated in the legend. The error bars represent the standard deviation

Dependence of the percolation threshold $\theta_p^*$ on the initial seed density $\rho$ differs significantly for the growing triangles, rhombuses, and hexagons. For the growing hexagons, $\theta_p^*$ decreases monotonically with $\rho$, while for the growing triangles and rhombuses decreases, reaches a minimum, increases, reaches a maximum and falls again for high values of $\rho$. The difference is most significant for lower initial seed densities, when the growing objects can reach larger sizes with larger influence on percolation.

All presented results suggest that the percolation threshold is most affected by the way of the object growth at low seed concentrations. This influence ceases when the value of $\rho$ tends to the percolation threshold for monomers.

**Acknowledgments** This work was supported by the Ministry of Education, Science, and Technological Development of the Republic of Serbia. Numerical simulations were run on the PARADOX supercomputing facility at the Scientific Computing Laboratory of the Institute of Physics Belgrade.

## Author contributions

Study conception and design: S. B. Vrhovac and Lj. Budinski-Petković; Analysis and interpretation of numerical data: D. Dujak, A. Karač and Z. M. Jakšić; Development of the numerical simulations: D. Dujak and A. Karač; Drafting of manuscript: S. B. Vrhovac and Lj. Budinski-Petković; Critical revision: S. B. Vrhovac, Lj. Budinski-Petković and Z. M. Jakšić

**Data Availability Statement** This manuscript has no associated data or the data will not be deposited. [Authors' comment: This is a theoretical study and there are no experimental data.]

## References

1. Dietrich Stauffer, Antonio Coniglio, and Mireille Adam, Gelation and critical phenomena,in Polymer Networks, edited by Karel Dušek (Springer Berlin Heidelberg, Berlin, Heidelberg, 1982) pp. 103–158
2. Paul Meakin, The growth of rough surfaces and interfaces. Phys. Rep. **235**, 189–289 (1993). https://doi.org/10.1016/0370-1573(93)90047-H
3. D. Stauffer, A. Aharony, *Introduction to percolation theory* (Taylor & Francis, London, 1994)
4. W. Lebrecht, P.M. Centres, A.J. Ramirez-Pastor, Analytical approximation of the site percolation thresholds for monomers and dimers on two-dimensional lattices. Physica A **516**, 133–143 (2019). https://doi.org/10.1016/j.physa.2018.10.023
5. Grzegorz Kondrat, Impact of composition of extended objects on percolation on a lattice. Phys Rev E **78**, 011101 (2008). https://doi.org/10.1103/PhysRevE.78.011101
6. V. Cornette, A.J. Ramirez-Pastor, F. Nieto, Dependence of the percolation threshold on the size of the percolating species, Physica A: Statistical Mechanics and its Applications**327**, 71–75 (2003). proceedings of the XIIIth Conference on Nonequilibrium Statistical Mechanics and Nonlinear Physics. https://doi.org/10.1016/S0378-4371(03)00453-9
7. Lj. Budinski-Petković, I. Lončarević, M. Petković, Z.M. Jakšić, S.B. Vrhovac, Percolation in random sequen-

tial adsorption of extended objects on a triangular lattice. Phys Rev E **85**, 061117 (2012). https://doi.org/10.1103/PhysRevE.85.061117
8. D. Dujak, A. Karač, Lj. Budinski-Petković, I. I Lončarević, Z. M. Jakšić, S. B. Vrhovac, Percolation in random sequential adsorption of mixtures on a triangular lattice. J Stat Mech **2019**, 113210 (2019). https://doi.org/10.1088/1742-5468/ab4588
9. J.W. Evans, Random and cooperative sequential adsorption. Rev Mod Phys **65**, 1281–1329 (1993). https://doi.org/10.1103/RevModPhys.65.1281
10. Vladimir Privman, Dynamics of nonequilibrium deposition. Colloids and Surfaces A: Physicochemical and Engineering Aspects **165**, 231–240 (2000). https://doi.org/10.1016/S0927-7757(99)00412-4
11. J. Talbot, G. Tarjus, P.R. Van Tassel, P. Viot, From car parking to protein adsorption: an overview of sequential adsorption processes. Colloids and Surfaces A: Physicochemical and Engineering Aspects **165**, 287–324 (2000). https://doi.org/10.1016/S0927-7757(99)00409-4
12. A. Cadilhe, N.A.M. Araújo, V. Privman, Random sequential adsorption: from continuum to lattice and pre-patterned substrates. J Phys **19**, 065124 (2007). https://doi.org/10.1088/0953-8984/19/6/065124
13. V. Cornette, A.J. Ramirez-Pastor, F. Nieto, Percolation of polyatomic species on a square lattice. Euro Phys J B Condensed Matter Complex Syst **36**, 391–399 (2003). https://doi.org/10.1140/epjb/e2003-00358-1
14. N. Vandewalle, S. Galam, M. Kramer, A new universality for random sequential deposition of needles. Euro Phys J B **14**, 407–410 (2000). https://doi.org/10.1007/s100510051047
15. Grzegorz Kondrat, Andrzej Pękalski, Percolation and jamming in random sequential adsorption of linear segments on a square lattice. Phys Rev E **63**, 051108 (2001). https://doi.org/10.1103/PhysRevE.63.051108
16. Grzegorz Kondrat, Zbigniew Koza, Piotr Brzeski, Jammed systems of oriented needles always percolate on square lattices. Phys Rev E **96**, 022154 (2017). https://doi.org/10.1103/PhysRevE.96.022154
17. M.G. Slutskii, LYu. Barash, YuYu. Tarasevich, Percolation and jamming of random sequential adsorption samples of large linear $k$-mers on a square lattice. Phys Rev E **98**, 062130 (2018). https://doi.org/10.1103/PhysRevE.98.062130
18. Federica Rampf, Ezequiel V. Albano, Interplay between jamming and percolation upon random sequential adsorption of competing dimers and monomers. Phys Rev E **66**, 061106 (2002). https://doi.org/10.1103/PhysRevE.66.061106
19. Piotr Adamczyk, Piotr Romiszowski, Andrzej Sikorski, A simple model of stiff and flexible polymer chain adsorption: the influence of the internal chain architecture. J Chem Phys **128**, 154911 (2008). https://doi.org/10.1063/1.2907715
20. Grzegorz Kondrat, Influence of temperature on percolation in a simple model of flexible chains adsorption. J Chem Phys **117**, 6662–6666 (2002). https://doi.org/10.1063/1.1505866
21. P. Longone, P.M. Centres, A.J. Ramirez-Pastor, Percolation of aligned rigid rods on two-dimensional square lattices. Phys Rev E **85**, 011108 (2012). https://doi.org/10.1103/PhysRevE.85.011108
22. E.J. Perino, D.A. Matoz-Fernandez, P.M. Pasinetti, A.J. Ramirez-Pastor, Jamming and percolation in random sequential adsorption of straight rigid rods on a two-dimensional triangular lattice. J Stat Mech **2017**, 073206 (2017). https://doi.org/10.1088/1742-5468/aa79ae
23. Joan Adler, Bootstrap percolation. Physica A **171**, 453–470 (1991). https://doi.org/10.1016/0378-4371(91)90295-N
24. S.R. Broadbent, J.M. Hammersley, Percolation processes. I: crystals and mazes. Math. Proc. Cambridge Philosophical Soc. **53**, 629–641 (1957). https://doi.org/10.1017/S0305004100032680
25. S.B. Santrs, I. Bose, Spiral site percolation on the square and triangular lattices. J. Phys. **25**, 1105–1118 (1992). https://doi.org/10.1088/0305-4470/25/5/018
26. Babak Nikoobakht, Mostafa A. El-Sayed, Preparation and growth mechanism of gold nanorods (nrs) using seed-mediated growth method. Chem. Materials **15**, 1957–1962 (2003). https://doi.org/10.1021/cm020732l
27. Anand Gole, Catherine J. Murphy, Seed-mediated synthesis of gold nanorods: role of the size and nature of the seed. Chem. Materials **16**, 3633–3640 (2004). https://doi.org/10.1021/cm0492336
28. Susan E. Habas, Hyunjoo Lee, Velimir Radmilovic, Gabor A. Somorjai, Peidong Yang, Shaping binary metal nanocrystals through epitaxial seeded growth. Nat. Materials **6**, 692–697 (2007). https://doi.org/10.1038/nmat1957
29. Samuel E. Lohse, The quest for shape control: a history of gold nanorod synthesis. Chem. Materials **25**, 1250–1261 (2013). https://doi.org/10.1021/cm303708p
30. Younan Xia, Kyle D. Gilroy, Hsin-Chieh. Peng, Xiaohu Xia, Seed-mediated growth of colloidal metal nanocrystals. Angewandte Chemie Int. Ed. **56**, 60–95 (2017). https://doi.org/10.1002/anie.201604731
31. Bappaditya Roy, S.B. Santra, First-order transition in a percolation model with nucleation and preferential growth. Phys. Rev. E **95**, 010101 (2017). https://doi.org/10.1103/PhysRevE.95.010101
32. Bappaditya Roy, S.B. Santra, Finite size scaling study of a two parameter percolation model: constant and correlated growth. Physica A **492**, 969–979 (2018). https://doi.org/10.1016/j.physa.2017.11.028
33. J. Carrey, J.-L. Maurice, Transition from droplet growth to percolation: Monte carlo simulations and an analytical model. Phys. Rev. B **63**, 245408 (2001). https://doi.org/10.1103/PhysRevB.63.245408
34. I. Lončarević, Lj. Budinski-Petković, D. Dujak, A. Karač, Z. M. Jakšić, and S. B. Vrhovac, The study of percolation with the presence of extended impurities, Journal of Statistical Mechanics: Theory and Experiment**2017**, 093202 (2017). http://stacks.iop.org/1742-5468/2017/i=9/a=093202
35. M.E.J. Newman, R.M. Ziff, Fast Monte Carlo algorithm for site or bond percolation. Phys. Rev. E **64**, 016706 (2001). https://doi.org/10.1103/PhysRevE.64.016706
36. I. Lončarević, Lj. Budinski-Petković, S.B. Vrhovac, Simulation study of random sequential adsorption of mixtures on a triangular lattice. Euro. Phys. J. E. **24**, 19–26 (2007). https://doi.org/10.1140/epje/i2007-10206-4

37. Lj. Budinski-Petković, S.B. Vrhovac, I. Lončarević, Random sequential adsorption of polydisperse mixtures on discrete substrates. Phys. Rev. E **78**, 061603 (2008). https://doi.org/10.1103/PhysRevE.78.061603
38. Lj Budinski-Petković, I Lončarević, Z M Jakšić, and S B Vrhovac, Jamming and percolation in random sequential adsorption of extended objects on a triangular lattice with quenched impurities, Journal of Statistical Mechanics: Theory and Experiment**2016**, 053101 (2016). http://stacks.iop.org/1742-5468/2016/i=5/a=053101
39. H. Markus Porto, Eduardo Roman, Critical packing fraction of rectangular particles on the square lattice. Phys. Rev. E **62**, 100–102 (2000). https://doi.org/10.1103/PhysRevE.62.100
40. Mitsunobu Nakamura, Percolational and fractal property of random sequential packing patterns in square cellular structures. Phys. Rev. A **36**, 2384–2388 (1987). https://doi.org/10.1103/PhysRevA.36.2384